Title
iConsol.js: JavaScript Implicit Finite-Difference Code for Nonlinear Consolidation and Secondary Compression

Journal
International Journal of Geomechanics, 17(6)

ISSN
1532-3641

Author
Brandenberg, Scott J

Publication Date
2017-06-01

DOI
10.1061/(asce)gm.1943-5622.0000843

Peer reviewed

iConsol.js: A Javascript Implicit Finite Difference Code for Nonlinear Consolidation and Secondary Compression

By, Scott J. Brandenberg, M. ASCE[1]

Abstract

An implicit finite difference code for nonlinear consolidation and secondary compression is developed and implemented in a publicly available Javascript web application. The rate of secondary compression is defined based on the distance in e-$\log_{10}(\sigma_v')$ space between a current point and a corresponding point on a reference secondary compression line (RSCL). Modeling secondary compression in this manner enables simultaneous occurrence of primary consolidation and secondary compression. The finite difference code is first verified by comparison with three benchmarks. The influence of secondary compression on settlement-versus-time is then studied, and shown to be important for thick and/or low permeability layers for which primary consolidation requires significant time. Overconsolidated soil is observed to result in an apparent increase in C_α with time, which is also observed in experimental data. Finally, secondary compression is shown to be capable of generating excess pore pressure in soils with impeded drainage boundaries.

Introduction

Terzaghi (1925) was the first to formulate the theory of one-dimensional consolidation for constant compressibility and hydraulic conductivity, and zero secondary compression. A primary benefit of Terzaghi's formulation is the ease of solving the governing second order partial differential equation. However, compressibility is known to depend on overconsolidation ratio and vertical effective stress, and hydraulic conductivity is known to depend on void ratio, both of which change during consolidation.

[1] Associate Professor and Vice Chair, Department of Civil and Environmental Engineering, University of California, Los Angeles, CA 90095-1593. Email: sjbrandenberg@ucla.edu

Furthermore, soil exhibits secondary compression behavior in which the void ratio constantly decreases even when effective stress is constant. Introducing nonlinear constitutive behavior and secondary compression complicates the governing differential equation, necessitating numerical solutions. Early approaches utilized rheological models involving a combination of sub-components, such as springs and dashpots, in various configurations [e.g., Taylor (1940), Taylor and Merchant (1942), Gibson and Lo (1961), Barden (1965)]. Though capable of being calibrated to match observed soil behavior, these models typically involved input parameters that were unfamiliar to users, and were not widely used (Perrone 1998). Computer codes developed to solve nonlinear consolidation problems using more traditional input parameters include Illicon (Mesri and Choi, 1985), CS1 (Rajot, 1992), CS2 (Fox and Berles, 1997), CONSOL97 (Perrone 1998), SETTLE3D (Rocscience 2007) as well as unnamed codes by Niemunis and Krieg (1996) and Yin and Graham (1996).

The various nonlinear codes vary significantly in the manner in which they treat secondary compression. Illicon incorporates secondary compression based on the assumption that "the end-of-primary void ratio-effective stress relationship is practically independent of the duration of the primary consolidation stage." Secondary compression settlement is then computed for the post-primary-consolidation phase based on the observation that C_α/C_c is a constant, where C_c is interpreted as the compressibility at the end of consolidation, and C_α is the coefficient of secondary compression. Similarly, SETTLE3D requires users to input a specific degree of consolidation (e.g., 95%) after which the solution is governed by secondary compression. A fundamental conclusion from these approaches is that secondary compression does not influence the evolution of excess pore pressures, and secondary compression becomes less important as the time required to reach the end of primary consolidation increases. CONSOL97 challenges this notion by including secondary compression concurrently with primary consolidation such that strains that occur during primary consolidation increase as the time required to reach the end of primary consolidation increases. Therefore, a thin laboratory specimen will exhibit less strain at the end of primary consolidation than a thicker field deposit, resulting in a scale effect. This is consistent with Bjerrum's (1967) time-line theory in which different consolidation lines would be measured for consolidation tests conducted with load stages of different duration.

A fundamental problem with nonlinear consolidation codes is that they are typically not readily available, and typically only utilized by the code developers. Perrone (1998) summarized 13 different nonlinear consolidation codes that include secondary compression, only one of which was commercially available. Fox (1999) used CS2 to develop chart solutions to make nonlinear consolidation solutions tangible to engineers without access to such codes. There is a significant need for a widely available, efficient code for routine use by researchers, engineers, and instructors.

This paper presents an implicit finite difference code for primary consolidation and secondary compression written in Javascript and deployed through an HTML user interface. The code is publicly available at www.uclageo.com/Consolidation, and is quick and efficient. The code is nonlinear in that it accounts for changes in hydraulic conductivity and compressibility as consolidation progresses. Furthermore, the code incorporates secondary compression in a manner that is based on soil state in e-$\log\sigma_v'$ space rather than depending on an arbitrary time reference. A discussion of secondary compression behavior is presented first, followed by development of the governing differential equation and the implicit finite difference scheme used to solve the equation. The code is then validated by comparing with benchmark solutions by Fox and Pu (2015) and an essentially linear problem is compared with Terzaghi's theory. The influence of overconsolidation ratio on the predicted rate of secondary compression is then discussed, and the influence of secondary compression on settlement versus time and excess pore pressures is then explored.

Shortcomings of Traditional Approach to Evaluating Secondary Compression

Secondary compression is traditionally evaluated by plotting void ratio, *e*, versus the logarithm of time, $\log_{10}(t)$, for a particular stage from a laboratory oedometer test (Fig. 1). Permitted adequate time, such curves have been observed to exhibit a linear secondary compression region in which the reduction in void ratio during one log-cycle of time is equal to the secondary compression index (C_α). Casagrande (1936) developed a procedure for evaluating laboratory oedometer curves to compute the coefficient of consolidation, c_v. This procedure identifies a time at the end of primary consolidation, t_p, for the purpose of computing the time at when 50% consolidation has completed. Primary consolidation is often interpreted as occurring before t_p whereas secondary compression occurs after t_p, which is termed the "traditional" approach herein.

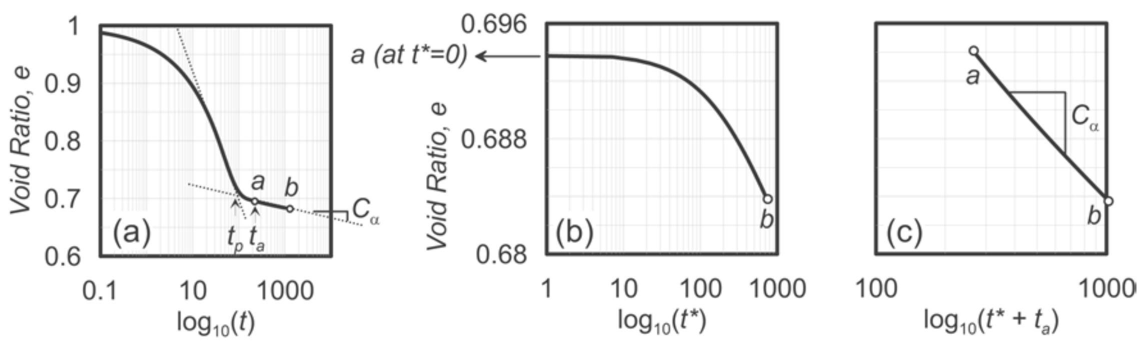

Figure 1. (a) Consolidation curve showing traditional primary consolidation and secondary compression behavior; (b) nonlinear secondary compression behavior when a vanishingly small load stage is applied and benchtop clock is reset such that $t^* = 0$ at Point a; (c) linear secondary compression when $t^* + t_a = 0$ at Point a.

The traditional approach for evaluating secondary compression is problematic for two fundamental reasons. First, primary consolidation and secondary compression occur simultaneously rather than occurring in distinct regions of time (e.g., Borja 1992, Niemunis et al. 1996, Yin and Graham 1996, Perrone 1998, Handy 2002, Leroueil 2006). Some secondary compression occurs prior to t_p, and some primary consolidation occurs after t_p. During a laboratory consolidation test, the amount of secondary compression that occurs before t_p may be small because the drainage path length is short and primary consolidation occurs rapidly. However, significantly more secondary compression may occur simultaneously with primary consolidation in the field, where drainage path lengths are much longer. The notion of t_p as a time dividing primary consolidation from secondary compression is therefore a false construct borne of convenience rather than rigor, and may result in errors when extrapolating laboratory observations to field behavior. Bjerrum (1967) explained this scale effect using a time-line idea in which different consolidation curves are associated with different amounts of time.

The second problem with the traditional approach to modeling secondary compression is that the benchtop clock provides an arbitrary time reference that is not fundamentally related to the state of the soil (e.g., Kutter and Sathialingam 1992). As an illustration, imagine that a vanishingly small load increment is applied at point *a* in Fig. 1 at the same instant that the benchtop clock is set to zero. Two different time references now exist; the symbol t denotes the time reference at the start of the load stage (Fig. 1a), whereas t^* denotes the clock that is reset at point *a*. The secondary compression rate does not change at point *a* because a vanishingly small load increment induces no change to the soil. However, the plot of e vs. $\log_{10}(t^*)$ is nonlinear simply because t* is not the correct time reference. Rather, the e vs. $\log_{10}(t^*)$ is concave downward, and asymptotically approaches a straight line with slope C_α as $t^* \rightarrow \infty$ (Fig. 1b). If t_a is added to t^*, linear secondary compression behavior is recovered (Fig. 1c). Applying a vanishingly small load increment would be an unreasonable experimental approach, but it nevertheless illustrates the arbitrariness of the benchtop clock. Furthermore, the concept explains why nonlinear secondary compression behavior is observed for overconsolidated soils, as discussed later.

An Alternative Approach to Secondary Compression

An alternative approach suggested by Kutter and Sathialingam (1992) defines the secondary compression rate based on position in e-log$_{10}$(σ_v') space rather than in e-log$_{10}$(t) space. Their formulation follows the visco-plasticity formulation of Perzyna (1963), but differs because plastic volumetric strains occur for all soil states rather than only for stress states on the yield surface. Kutter and Sathialingam implemented this procedure in a Cam-Clay type plasticity model, but the implementation herein focuses only on one-dimensional consolidation and therefore utilizes different terminology. Mapping from the traditional e-log$_{10}$(t) space to e-log$_{10}$(σ_v') follows Bjerrum's time-line notion as illustrated in Fig. 2. The notion of a reference secondary compression line(RSCL) is introduced, where the RSCL is associated with a specific reference time, t_{ref}, as well as a single point on the line defined by a reference void ratio and vertical effective stress, $e_{c\alpha,ref}$, and $\sigma_v'{}_{c\alpha,ref}$, respectively. The RSCL may be selected to be coincident with the normal consolidation line (NCL), in which case $t_{ref} = t_p$. The NCL and RSCL are assumed to be parallel, which is consistent with experimental observations that the ratio C_α/C_c is constant (Mesri and Godlewski 1977).

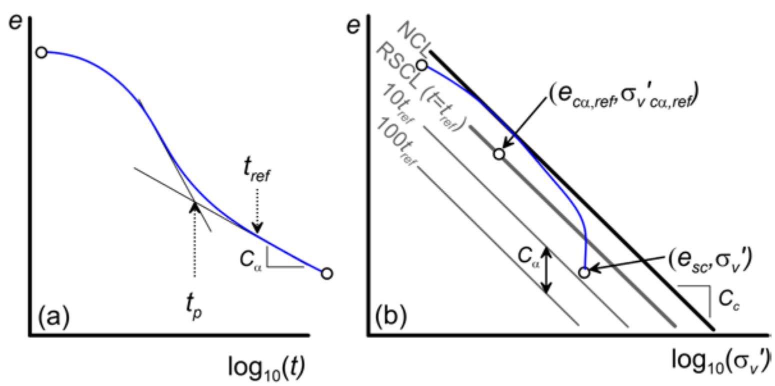

Figure 2. Consolidation curve for an initially lightly overconsolidated soil: (a) in e-log$_{10}$(t) space; (b) in e-log$_{10}$(σ'_v) space.

The load stage in Fig. 2a follows a characteristic e-log$_{10}$(t) consolidation curve for an initially lightly overconsolidated soil, and Fig. 2b shows the corresponding stress path in e-log$_{10}$(σ_v') space. The stress path drops below the NCL before the end of primary consolidation because some secondary compression is assumed to occur during primary consolidation. The soil eventually reaches a condition wherein primary consolidation is negligible, resulting in essentially a straight line in e-$\log_{10}(t)$ space with a slope C_α, and a vertical line in e-$\log_{10}(\sigma_v')$ space. The void ratio at which the stress path crosses the RSCL is $e_{c\alpha,ref} - C_c\log(\sigma_v'/\sigma_v'_{c\alpha,ref})$. Assuming secondary compression controls the void ratio change during the essentially linear portion of the e-$\log_{10}(t)$ curve, the void ratio during secondary compression, e_{sc}, is defined by Eq. 1.

$$e_{sc} = e_{c\alpha,ref} - C_c \log_{10}\left(\frac{\sigma_v'}{\sigma_v'_{c\alpha,ref}}\right) - C_\alpha \log_{10}\left(\frac{t}{t_{ref}}\right) \tag{1}$$

Differentiating Eq. 1 with respect to t results in the rate of change of void ratio due to secondary compression, as shown in Eq. 2, where $\alpha = C_\alpha/\ln(10)$.

$$\dot{e}_{sc} = -\frac{C_\alpha}{\ln(10)\cdot \mathrm{t}} = -\frac{\alpha}{t} \tag{2}$$

Solving Eq. 1 for t, substituting into Eq. 2 and noting that $\dot{\varepsilon}_{v,sc} = -\dot{e}_{sc}/(1+e)$ results in the secondary compression volumetric strain rate given by Eq. 3.

$$\dot{\varepsilon}_{v,sc} = \frac{\alpha}{t_{ref}(1+e)} \exp\left(\frac{e - e_{c\alpha,ref}}{\alpha} + \frac{C_c}{\alpha}\log_{10}\left(\frac{\sigma_v'}{\sigma_v'_{c\alpha,ref}}\right)\right) \tag{3}$$

Eq. 3 defines the secondary compression volumetric strain rate at any point in e-$\log_{10}(\sigma_v')$ space based on the material constants t_{ref}, $e_{c\alpha,ref}$, $\sigma_v'_{c\alpha,ref}$, and c_α, all of which can be measured in a traditional oedometer test for which the secondary compression behavior is linear in e-$\log_{10}(t)$ space. This formulation permits simultaneous occurrence of secondary compression with primary consolidation by simply integrating the secondary compression strain rate for a particular consolidation increment. Furthermore, Eq. 3 is formulated based on the state of the soil rather than an arbitrary benchtop clock. The approach therefore overcomes the two fundamental shortcomings of the traditional approach to quantifying secondary compression that were described in the previous section. Specifically, the secondary compression strain rate no longer depends on a specific time reference, and can easily be included during primary consolidation.

Derivation of Differential Equation Governing Nonlinear Consolidation

Consider a layer of "uniform" saturated clay of thickness H with an initial vertical effective stress at the surface q_o exposed to a vertical pressure increment Δq (Fig. 3). In this context, a "uniform" clay has a constant specific gravity, G_s, constant e-$\log_{10}(k)$ and e-$\log_{10}(\sigma_v')$ relationships, constant C_α, and one of the following is constant: overconsolidation ratio, OCR, initial void ratio, e_o, or maximum past pressure, σ_p'. The initial water table is assumed hydrostatic. The top and bottom of the layer may be either free draining or impermeable, resulting in three possible drainage conditions: double drained, single drained through the top, or single drained through the bottom.

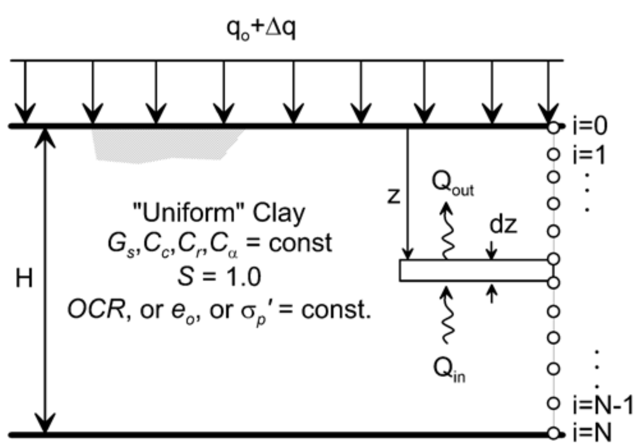

Figure 3. A uniform soil layer of initial thickness H with initial vertical effective stress q_o at the top exposed to a vertical stress change Δq illustrating node numbering for the finite difference scheme.

Derivation of the governing differential equation proceeds by additive decomposition of the volumetric strain rate, $\dot{\varepsilon}_v$, into components from primary consolidation, $\dot{\varepsilon}_{v,pc}$, and secondary compression, $\dot{\varepsilon}_{v,sc}$, as indicated in Eq. 4. The expression for $\dot{\varepsilon}_{v,sc}$ is given by Eq. 3, whereas the expression for $\dot{\varepsilon}_v$ is obtained from Darcy's law, and $\dot{\varepsilon}_{v,pc}$ is derived from rate-independent elasto-plasticity.

$$\dot{\varepsilon}_v = \dot{\varepsilon}_{v,pc} + \dot{\varepsilon}_{v,sc} \tag{4}$$

Expression for $\dot{\varepsilon}_v$ by Darcy's law

Flow out of and into an infinitesimal element of porous material is shown in Fig. 3 and the rate of flow is given by Eqs. 5 and 6.

$$\dot{Q}_{out} = k_z i_z dxdy \tag{5}$$

$$\dot{Q}_{in} = k_{z+dz} i_{z+dz} dxdy \tag{6}$$

Noting that $k_{z+dz} = k_z + (\partial k/\partial z)dz$, $i_z = 1/\gamma_w \cdot \partial u/\partial z$, and $i_{z+dz} = i_z + (\partial i/\partial z)dz$, , and neglecting the dz^2 term arising from multiplication of k_{z+dz} and i_{z+dz}, the volumetric strain rate is defined in Eq. 7. The z-subscripts have been omitted from Eq. 7, though it is implied that this equation holds at a particular depth.

$$\dot{\varepsilon}_v = \frac{\left(\dot{Q}_{out} - \dot{Q}_{in}\right)}{dxdydz} = -\frac{1}{\gamma_w}\left(k\frac{\partial^2 u}{\partial z^2} + \frac{\partial u}{\partial z}\frac{\partial k}{\partial z}\right) \tag{7}$$

Many experimental studies have shown that void ratio is linearly related to the logarithm of hydraulic conductivity (e.g., Taylor 1948, Tavenas et al. 1983, Mesri and Choi 1985, Fox 1999). Therefore, the constitutive relation shown in Fig. 4 is utilized, and is characterized by the slope of the e-$\log_{10}(k)$ relation, C_k, and a reference point ($e_{k,ref}$, k_{ref}) lying anywhere on the line.

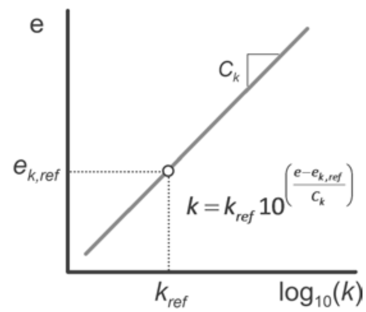

Figure 4. Constitutive relation for hydraulic conductivity.

Expression for $\dot{\varepsilon}_{v,pc}$ *by elasto-plasticity*

Compressibility due to primary consolidation is governed by conventional consolidation theory, as shown in Fig. 5, where $\sigma_{v'ref}$ and e_{ref} define a point on the NCL, C_c and C_r are the slopes of the NCL and unload-reload lines, respectively, and σ_p' is the maximum past pressure. The NCL is considered to be a stationary yield surface, and a stress state is not permitted to lie to the right of the NCL.

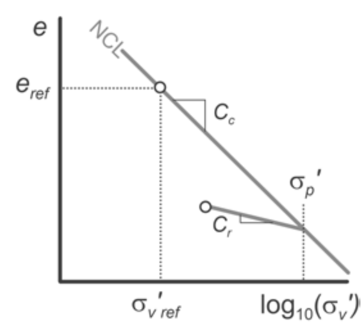

Figure 5. Constitutive relation for compressibility.

The maximum past pressure, σ_p', is a variable that evolves as loading progresses beyond the initial value of σ_p', and σ_v' can never be larger than σ_p'. The value of σ_p' is computed based on the current stress condition by Eq. 8.

$$\log_{10}\left(\sigma_p^{'}\right)=\frac{e_{ref}-e+C_c\log_{10}\left(\sigma_{v,ref}^{'}\right)-C_r\log_{10}\left(\sigma_v^{'}\right)}{C_c-C_r} \tag{8}$$

The change in void ratio for a particular load increment depends on whether the specimen is normally consolidated, begins and remains over-consolidated, or begins overconsolidated and becomes normally consolidated, as defined in Eq. 9. A secant value of the coefficient of compressibility can then be computed as $a_v = -de/d\sigma_v'$ for a particular load increment.

$$\begin{aligned}
de &= C_c\log\left(\frac{\sigma_v'+d\sigma_v'}{\sigma_v'}\right) && \textit{if}\quad \sigma_v'=\sigma_p' && \text{Normally Consolidated (NC)}\\
de &= C_r\log\left(\frac{\sigma_v'+d\sigma_v'}{\sigma_v'}\right) && \textit{if}\quad \sigma_v'+\mathrm{d}\sigma_v'<\sigma_p' && \text{Overconsolidated (OC)}\\
de &= C_r\log\left(\frac{\sigma_p'}{\sigma_v'}\right)+C_c\log\left(\frac{\sigma_v'+d\sigma_v'}{\sigma_p'}\right) && \textit{otherwise} && \text{Initially OC, Becomes NC}
\end{aligned} \tag{9}$$

The volumetric strain rate due to primary consolidation is expressed in terms of the coefficient of compressibility as indicated in Eq. 10, where, $du/dt = -d\sigma_v'/dt$, and $\varepsilon_{v,pc} = -de/(1+e)$ (i.e., compressive volumetric strain is positive).

$$\dot{\varepsilon}_{v,pc}=-\frac{a_v}{1+e}\frac{\partial u}{\partial t} \tag{10}$$

Governing differential equation

Substituting Eqs. 3, 7, and 10 into Eq. 4 results in the governing differential equation for one-dimensional consolidation of an elasto-plastic porous solid (Eq. 11), including nonlinear compressibility and permeability properties along with the effects of secondary compression.

$$\frac{1}{\gamma_w}\left(k\frac{\partial^2 u}{\partial z^2}+\frac{\partial u}{\partial z}\frac{\partial k}{\partial z}\right)-\frac{a_v}{1+e_o}\frac{\partial u}{\partial t}+\frac{\alpha}{t_{ref}\left(1+e_o\right)}\exp\left(\frac{e-e_{c\alpha,ref}}{\alpha}+\frac{C_c}{\alpha}\log\left(\frac{\sigma_v'}{\sigma_v'{}_{c\alpha,ref}}\right)\right)=0 \tag{11}$$

Finite Difference Solution Scheme

An implicit finite difference scheme utilizing the midpoint rule (Crank and Nicolson, 1947) is adopted to solve Eq. 11, where *i* denotes discretization in space (Fig. 3) and *j* denotes discretization in time with $\Delta t_j = t_j - t_{j-1}$. In general, values of the internal variables are different at the beginning and end of the time step. Incremental strains are computed based on the values of the variables at the beginning and those at the end, and the average of these strains is utilized in implementing the midpoint rule. Note that $(a_v)_{i,j}$ is the secant value of $\boldsymbol{a_v}$ for the time step computed as $de_{i,j}/(\sigma'_{v\,i,j} - \sigma'_{v\,i,j-1})$. The value of Δz is computed as $0.5\cdot(z_{i+1,j} - z_{i-1,j})$, except at the top and bottom boundaries, where Δz is computed as $z_{1,j} - z_{0,j}$ and $z_{N,j} - z_{N-1,j}$, respectively. The resulting incremental form is indicated in Eq. 12, where $R_{i,j}$ is a residual that must be minimized.

$$
\begin{aligned}
0 \approx R_{i,j} = & \frac{(a_v)_{i,j}}{1+e_{i,j-1}} \frac{u_{i,j}-u_{i,j-1}}{t_j - t_{j-1}} + \frac{k_{i,j}}{2}\left[\frac{\left(u_{i+1,j} - 2u_{i,j} + u_{i-1,j}\right)}{\Delta z^2_{i,j}}\right] + \frac{k_{i,j-1}}{2}\left[\frac{\left(u_{i+1,j-1} - 2u_{i,j-1} + u_{i-1,j-1}\right)}{\Delta z^2_{i,j-1}}\right] + \\
& + \frac{1}{2}\left[\frac{\left(u_{i+1,j} - u_{i-1,j}\right)\left(k_{i+1,j} - k_{i-1,j}\right)}{\Delta z^2_{i,j}} + \frac{\left(u_{i+1,j-1} - u_{i-1,j-1}\right)\left(k_{i+1,j} - k_{i-1,j}\right)}{\Delta z^2_{i,j-1}}\right] + \\
& + \frac{0.5\alpha}{t_{ref}\left(1+e_{i,j-1}\right)}\left[\exp\left(\frac{e_{i,j} - e_{c\alpha,ref}}{\alpha} + \frac{C_c}{\alpha}\log\left(\frac{(\sigma_v{}')_{i,j}}{\sigma_v{}'_{c\alpha,ref}}\right)\right) + \exp\left(\frac{e_{i,j-1} - e_{c\alpha,ref}}{\alpha} + \frac{C_c}{\alpha}\log\left(\frac{(\sigma_v{}')_{i,j-1}}{\sigma_v{}'_{c\alpha,ref}}\right)\right)\right]
\end{aligned}
\tag{12}
$$

Equation 12 contains i+1 and i-1 terms for $\boldsymbol{u}$, and $\boldsymbol{k}$, which requires consideration of boundary conditions at the top and bottom of the domain (i.e., when i=0 or i=N). Values of hydraulic conductivity that lie beyond the domain are set to $k_{-1,j} = k_{0,j}$ and $k_{N+1,j} = k_{N,j}$. For a free-draining boundary at the top $u_{i-1,j} = u_{0,j} = 0$, and at the bottom $u_{N+1,j} = u_{N,j} = 0$. For an impermeable drainage boundary, a zero flow condition is obtained by forcing the hydraulic gradient to be zero by setting $u_{-1,j} = u_{0,j}$ at the top or $u_{N+1,j} = u_{N,j}$, and subsequently solving for the pressure at the impermeable boundary.

The solution proceeds by first initializing $\boldsymbol{\sigma_v'}$, $\boldsymbol{e}$, $\boldsymbol{a_v}$, $\boldsymbol{k}$, and $\boldsymbol{\Delta z}$ for pre-load conditions. The initial element height is set to H/(N-1). The initial vertical effective stress at the top of the layer is q_o. The known initial profile of either $\boldsymbol{e}$, ***OCR***, or $\boldsymbol{\sigma_p'}$ is then used to initialize the remaining internal variables. If the initial profile of $\boldsymbol{e}$ is assumed constant, the saturated unit weight is computed as $\gamma_{sat} = \gamma_w(\boldsymbol{G_s}+\boldsymbol{e})/(1+\boldsymbol{e})$, and the vertical total stress profile is computed by integrating this unit weight with depth. If the initial profile of ***OCR*** or $\boldsymbol{\sigma_p'}$ is set to be constant, the initialization procedure is slightly more complicated because γ_{sat} varies with depth because $\boldsymbol{e}$ is not constant. First, the value of $\boldsymbol{e_o}$ at the top boundary is computed using Eq. 9 after substituting $\sigma_{vo}' = q_o$, and the value of γ_{sat} is computed at the surface. The value of γ_{sat} is then computed at the i+1 node by iteration since γ_{sat} depends on void ratio, and hence on vertical effective stress. The average value of γ_{sat} is then used to compute effective stress at the i+1 node and the procedure is repeated to the bottom of the domain.

The next step is to define a time vector based on the desired number of increments, N_{time}, and the maximum value of time to be analyzed, t_{max}. Following initialization, values of c_v are computed at each node, and the maximum value is selected. The first time increment is selected to be $t_{min} = \alpha \cdot \Delta z^2/c_v$ where $\alpha = 0.025$, and Δz *is the initial element height*. Note that explicit integration finite difference algorithms require $\alpha<0.5$ for numerical stability when solving linear problems (e.g., Fox and Berles 1997). The value $\alpha = 0.025$ was found to provide a reasonable initial starting point, and avoid problems associated with very large strains at the top and bottom elements that may occur during the first time step. The time vector is then set to be logarithmically distributed between t_{min} and t_{max}.

The solution for the j components of $\boldsymbol{u}$ proceeds by making an initial guess by setting the j components of $\boldsymbol{a_v}$, $\boldsymbol{k}$, $\boldsymbol{\Delta z}$, $\boldsymbol{e}$, and $\boldsymbol{\sigma_v'}$ equal to the j-1 components, and algebraically isolating the j components of $\boldsymbol{u}$ in Eq. 12. The system of equations can be expressed as [**A**]{**u**}={**x**}, where **A** is a tridiagonal matrix. Components of **A** and **x** are defined by Eq. 13. The guess values are then computed as

$\mathbf{u} = \mathbf{A}^{-1}\mathbf{x}$, and $\mathbf{A}^{-1}$ is computed using an efficient tridiagonal matrix algorithm (Thomas 1949), wherein the number of computations scales linearly with the dimension of **A**, whereas Gaussian elimination scales with the cube of the dimension of **A**.

$$
\begin{aligned}
&\left[A_{i,i}\right]_j = \frac{a_{vi,j}}{1+e_{i,j-1}} + \frac{k_{i,j}\cdot\Delta t}{\gamma_w\cdot\Delta z_{i,j}^2} \\
&\left[A_{i,i-1}\right]_j = -\frac{0.5\cdot\Delta t}{\gamma_w\cdot\Delta z_{i,j}^2}\left[k_{i,j} - 0.25\cdot\left(k_{i+1,j}-k_{i-1,j}\right)\right] \\
&\left[A_{i,i+1}\right]_j = -\frac{0.5\cdot\Delta t}{\gamma_w\cdot\Delta z_{i,j}^2}\left[k_{i,j} + 0.25\cdot\left(k_{i+1,j}-k_{i-1,j}\right)\right] \\
&x_{i,j} = \frac{a_{vi,j-1}\cdot u_{i,j-1}}{1+e_{i,j-1}} + \frac{0.5\cdot k_{i,j-1}\cdot\Delta t_j}{\gamma_w\cdot\Delta z_{i,j-1}^2}\left(u_{i-1,j-1} - 2\cdot u_{i,j-1} + u_{i+1,j}\right) + \frac{0.125\cdot\Delta t_j}{\gamma_w\cdot\Delta z_{i,j-1}^2}\left(u_{i+1,j-1}-u_{i-1,j-1}\right)\left(k_{i+1,j-1}-k_{i-1,j-1}\right) + \\
&\qquad + \frac{0.5\cdot\alpha\cdot\Delta t_j}{t_{ref}\cdot\left(1+e_{i,j-1}\right)}\left[\exp\left(\frac{e_{i,j-1}-e_{c\alpha,ref}}{\alpha} + \frac{C_c}{\alpha}\log\left(\frac{\sigma_{vi,j-1}}{\sigma_{c\alpha,ref}}\right)\right) + \exp\left(\frac{e_{i,j}-e_{c\alpha,ref}}{\alpha} + \frac{C_c}{\alpha}\log\left(\frac{\sigma_{vi,j}}{\sigma_{c\alpha,ref}}\right)\right)\right]
\end{aligned}
\tag{13}
$$

Following calculation of the trial values of ***u***, residuals are computed using Eq. 12. If the maximum of the absolute value of any residual exceeds a tolerance, the values of ***u*** are updated using Newton-Raphson iteration. The values of d***R***/d***u*** must be computed for the Newton-Raphson scheme, and are defined by the partial derivative chain rule in Eq. 14. Expressions for the partial derivatives are provided in the appendix.

$$
\begin{aligned}
&\frac{dR_{i,j}}{du_{i,j}} = \frac{\partial R_{i,j}}{\partial u_{i,j}} + \frac{\partial R_{i,j}}{\partial \sigma_{v_{i,j}}}\frac{\partial \sigma_{vi,j}}{\partial u_{i,j}} + \frac{\partial R_{i,j}}{\partial k_{v_{i,j}}}\frac{\partial k_{i,j}}{\partial e_{v_{i,j}}}\frac{\partial e_{v_{i,j}}}{\partial u_{i,j}} + \frac{\partial R_{i,j}}{\partial a_{v_{i,j}}}\frac{\partial a_{vi,j}}{\partial \sigma_{v_{i,j}}}\frac{\partial \sigma_{v_{i,j}}}{\partial u_{i,j}} + \frac{\partial R_{i,j}}{\partial \Delta z_{i,j}}\frac{\partial \Delta z_{i,j}}{\partial e_{i,j}}\frac{\partial e_{i,j}}{\partial u_{i,j}} + \frac{\partial R_{i,j}}{\partial e_{i,j}}\left(\frac{\partial e_{i,j}}{\partial u_{i,j}} + \frac{\partial e_{i,j}}{\partial \sigma_{v_{i,j}}}\frac{\partial \sigma_{v_{i,j}}}{\partial u_{i,j}}\right) \\
&\frac{dR_{i,j}}{du_{i-1,j}} = \frac{\partial R_{i,j}}{\partial u_{i-1,j}} + \frac{\partial R_{i,j}}{\partial k_{i-1,j}}\frac{\partial k_{i-1,j}}{\partial e_{i-1,j}}\frac{\partial e_{i-1,j}}{\partial u_{i-1,j}} \\
&\frac{dR_{i,j}}{du_{i+1,j}} = \frac{\partial R_{i,j}}{\partial u_{i+1,j}} + \frac{\partial R_{i,j}}{\partial k_{i+1,j}}\frac{\partial k_{i+1,j}}{\partial e_{i+1,j}}\frac{\partial e_{i+1,j}}{\partial u_{i+1,j}}
\end{aligned}
\tag{14}
$$

After assembling the tridiagonal d***R***/d***u*** matrix, the values of ***u*** are updated using Eq. 15, where the superscript <*m*> denotes the m^{th} iteration. Updated values of $\boldsymbol{\sigma_v'}$, $\boldsymbol{a_v}$, $\boldsymbol{k}$, and $\boldsymbol{\Delta z}$ are computed, and a new residual vector $\boldsymbol{R}^{<m>}$ is computed. Iterations proceed until the maximum of the absolute value of ***R*** is less than the tolerance. Note that ***R*** is the error in strain increments, and is therefore dimensionless. The convergence rate for the algorithm is approximately linear, and accurate solutions can be computed on a personal computer in less than a second for 500 time steps and 100 elements.

$$u^{\langle m \rangle} = u^{\langle m-1 \rangle} - \left(\frac{dR}{du}^{\langle m-1 \rangle} \right)^{-1} R^{\langle m-1 \rangle} \quad (15)$$

Comparison with Benchmark Solutions

Three benchmark solutions are utilized to verify implementation of the nonlinear primary consolidation portion of the code (such benchmarks are not available for non-zero secondary compression). The first two were presented by Fox and Pu (2015) for the expressed purpose of verifying nonlinear consolidation codes. The third involves a comparison with Terzaghi's (1926) one-dimensional consolidation theory for a case in which a_v and k (and therefore c_v) are essentially constant. Input parameters for the benchmark cases are provided in Table 1. Fox and Pu (2015) utilized the same soil profile for Benchmark 1 and 2, with Benchmark 1 corresponding to a profile of normally consolidated soil and Benchmark 2 corresponding to a profile of initially overconsolidated soil that subsequently becomes normally consolidated as a result of loading. For Benchmark 3, the compressibility and permeability remain essentially constant throughout because (i) the specimen height is very small, self-weight of the soil is negligible, therefore compressibility is constant, (ii) the load increment very small, the void ratio change is negligible, therefore a_v and k remain essentially constant during loading, (iii) the value of C_k is large resulting in essentially constant hydraulic conductivity, and (iv) C_α is set to zero to facilitate a comparison of primary consolidation only.

Figure 6 shows comparisons between benchmark solutions for nonlinear consolidation codes presented by Fox and Pu (2015) with those computed using the implicit algorithm. Agreement is good for both benchmarks, though there are some visible differences in the pore pressure and void ratio isochrones and minor differences in the settlement versus time plot for benchmark 1. The cause of these small differences is not currently understood, but is not due to the temporal or spatial discretization. Increasing N_{time} or N_{ele} from 100 to 500 or 1000 steps results in essentially no difference in the computed solutions. The important behavior trends are identical between the two solutions, and they are similar enough to conclude that the validation study is successful.

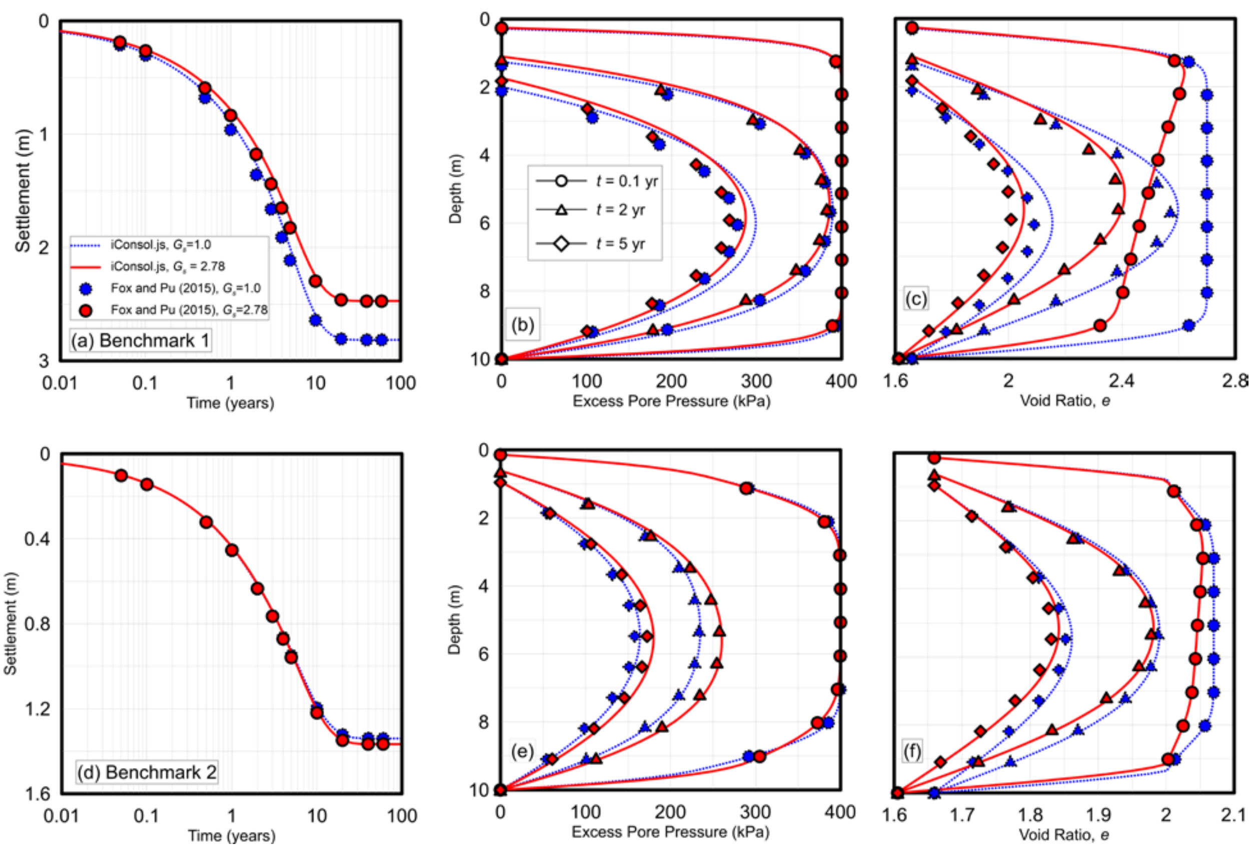

Figure 6. Comparison of Fox and Pu (2015): (a) Benchmark 1 settlement versus time; (b) Benchmark 1 excess pore pressure versus depth; (c) Benchmark 1 void ratio versus depth; (d) Benchmark 2 settlement versus time; (e) Benchmark 2 excess pore pressure versus depth; (f) Benchmark 2 void ratio versus depth.

Figure 7 shows comparisons of U_{ave} vs. T_v and U_z vs. Z for benchmark 3. Excellent agreement is achieved between Terzaghi's solution and the numerical solutions for the U_{ave} vs. T_v curve for all values of N_{time}. Furthermore excellent agreement is achieved for U_z vs. Z for all cases except N_{time} = 20, where errors appear in the isochrones near the drainage boundaries. In all cases, the solutions required a computation time of only a fraction of a second, so the poor performance at N_{time} = 20 is of little practical consequence. Rather, the purpose of including this solution is to demonstrate the stability of the implicit integration algorithm. Explicit algorithms that utilize the forward Euler method suffer instability problems when $\Delta t > 0.5\Delta z^2/c_v$ (e.g., Fox and Berles 1997), whereas the implicit algorithm used herein is stable and accurate for very large time steps, thereby improving computational efficiency.

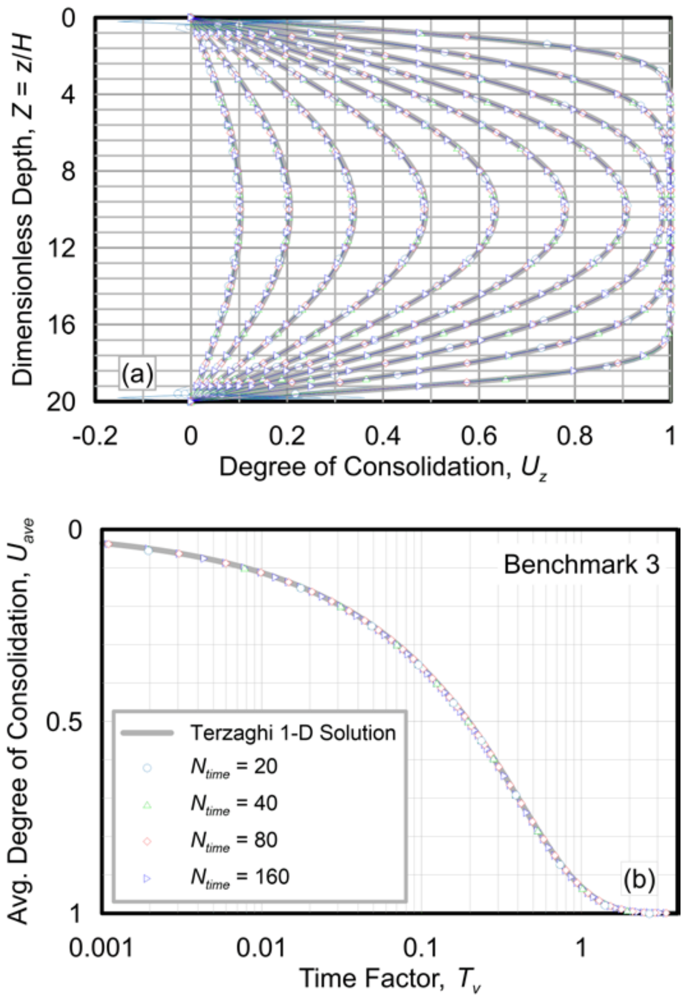

Figure 7. Comparison with Terzaghi's 1D consolidation theory for Benchmark 3: (a) dimensionless depth versus degree of consolidation; (b) time versus degree of consolidation.

Influence of Secondary Compression on Settlement

Because secondary compression occurs simultaneously with primary consolidation, it influences settlement rate in a manner that depends on the rate of primary consolidation. All other factors being equal, a soil layer that consolidates slowly will exhibit more secondary compression during primary consolidation than a soil layer that consolidates quickly. Figure 8 shows normalized settlement, $S/S_{c,ult}$, versus normalized time, t/t_{50}, for a soil with the same properties as Benchmark 1, but with H = 0.02, 0.2, 2.0, and 20.0m, and with C_α = 0.0 and 0.025. This range of thickness values was selected because 0.02m is a common thickness for a laboratory oedometer specimen, while 20m is in the reasonable range for a thick natural clay deposit. The values of $S_{c,ult}$ and t_{50} were computed from the analyses with C_α = 0 to identify the settlement arising only from primary consolidation. In defining the secondary compression parameters, the NCL for Benchmark 1 was assumed to have been derived from a laboratory oedometer test. The value of t_{ref} was therefore computed at the end of primary consolidation for the 0.02m thick soil layer using Casagrande's procedure. Because t_{ref} was computed at the end of primary consolidation, the RSCL is coincident with the NCL and values of $\sigma_{v'c\alpha,ref}$ and $e_{c\alpha,ref}$ were selected to be identical to $\sigma_{v}'_{,ref}$ and $e_{\sigma v,ref}$, respectively, as included in Fig. 8.

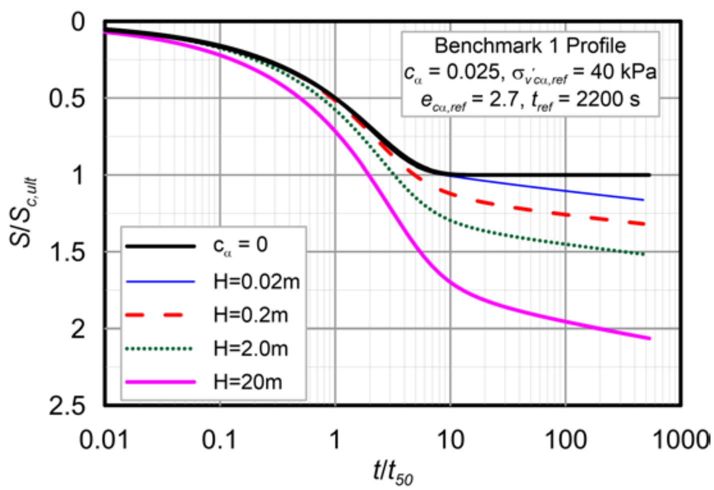

Figure 8. Normalized settlement versus time for soil layers with various thickness.

For C_α = 0, the dimensionless settlement plots are essentially identical, regardless of layer thickness. Although it appears only a single line is plotted for C_α = 0 in Fig. 8, lines are in fact plotted for all four thicknesses, but the differences between the lines are smaller than the line thicknesses. However, for C_α = 0.025, settlement increases as layer thickness increases. For H=0.02m, very little secondary compression occurs during primary consolidation, and conceptualizing secondary compression and primary consolidation as occurring in distinct regions of time (i.e., the traditional interpretation) is reasonable. However, the rate of primary consolidation is much slower for thicker soil layers, therefore more secondary compression occurs during primary consolidation, rendering the traditional interpretation increasingly erroneous as *H* increases. For *H*=20m, the settlement at the “end” of primary consolidation is approximately $1.8 \cdot S_{c,ult}$. Utilizing the traditional interpretation would therefore significantly under-predict settlement at the “end” of primary consolidation.

Influence of OCR on Secondary Compression

Overconsolidated soil has long been recognized as exhibiting less secondary compression than normally consolidated soil (e.g., Mesri and Ajlouni 2007, Lambrechts et al. 2004). Furthermore, studies have indicated that the slope of the secondary compression line in e-$\log_{10}(t)$ space increases with time for overconsolidated soil, whereas it is linear for normally consolidated soil (Mesri et al. 1997, Fox et al. 1992). Fox et al. (1992) postulated the existence of “tertiary compression” in peat samples due to an increase in the rate of secondary compression with time. The vanishingly small load stage in Fig. 1 also exhibited an apparent increase in C_α with increasing $\log_{10}(t)$ when the incorrect time reference was used.

To explore the influence of OCR on nonlinearity in secondary compression in e-$\log_{10}$(t) space, consider the data presented by Mesri et al. (1997) for load stage T15 and corresponding prediction in Fig. 9. Input parameters for the prediction were selected based on Figures 4, 6, 7, and 8 in Mesri et al., and are summarized in Table 2. This particular load stage began with q_o = 24 kPa, and finished with 36 kPa, which also happens to be the maximum past pressure. The slope of the consolidation curve in this region was steeper than the unload-reload region, but less steep than the virgin compression region. A secant slope for C_r was computed as 3.0 in this region. The secondary compression behavior for this load stage was nonlinear, so the normally consolidated load stage T14 was used to select C_α because its secondary compression was much more linear. Furthermore, tp was found to be 40 min. for stage T14 based on pore pressure measurements at the bottom of the single-drained specimen, and t_{ref} was computed as being equal to t_p in this case.

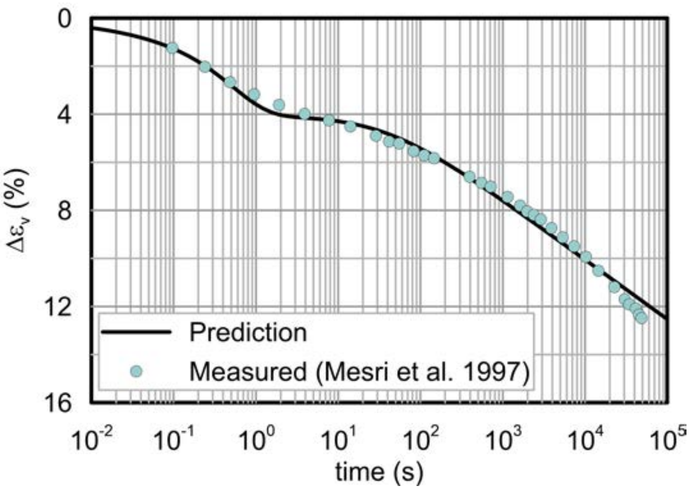

Figure 9. Measured and predicted volumetric strain versus time for Load Stage T15 imposed on a peat specimen by Mesri et al. (1997).

The measurements exhibit an initial consolidation stage followed by a secondary compression stage in which the slope of the data in e-$\log_{10}(t)$ space increases with time. The prediction exhibits the same qualitative behavior, and agrees quite well with the measurements. The prediction exhibits a flatter slope immediately after the end of primary consolidation. Furthermore, the data exhibit a steeper slope near the end of the load stage. A number of factors may be at work in explaining the observed behavior, including biological degradation, micromechanical behavior of the fibers, or others. However, a portion of the nonlinear behavior is clearly explained by defining secondary compression rate as a function of soil state (i.e., in e-$\log_{10}(\sigma_v')$ space) rather than using an arbitrary time reference.

Influence of Secondary Compression on Pore Pressure

In a free-draining condition, the plastic volumetric strains that accumulate during secondary compression manifest as total volumetric strain, and hence soil settlement. However, plastic volumetric strains arise from secondary compression regardless of drainage conditions, and therefore may result in an increase in excess pore pressure (e.g., Borja 1992). To illustrate this concept, an isotropic consolidation test was performed on a specimen of reconstituted Sherman Island peat from the Sacramento / San Joaquin Delta, after which the drainage taps were closed and pore pressure was measured. This sample was taken from a depth of 3.0m from a site on Sherman Island where a field test was conducted (Reinert et al. 2013), and Shafiee (2016) measured consolidation characteristics reported in Table 2. The sample was first mixed as a slurry, and subsequently consolidated in a Shelby tube to a vertical stress of 10 kPa. The specimen was then extruded, trimmed, and placed in a triaxial cell. The isotropic consolidation test involved first consolidating the sample to 10 kPa in the device. Subsequently, the specimen was consolidated to 20 kPa in stage 1, and 40 kPa in stage 2. Drainage was provided through the top of the specimen while pore pressure was monitored at the bottom to ascertain the time at the end of primary consolidation, which can be difficult to measure based on volume change versus time for soils with high secondary compression. The drainage tap was then closed at the end of consolidation in stage 2, and the pore pressure was monitored.

The volumetric strain versus time measured in stage 1 is presented in Fig. 10 up to a time near 70,000 seconds at which point the burette filled with water thereby preventing further expulsion of water from the peat. Water was subsequently removed from the burette, and consolidation progressed to the final desired effective stress. However, the volume change-versus-time relationship could no longer be plotted due to the interruption. A prediction using the one-dimensional consolidation code is also shown. To facilitate a comparison between an isotropic consolidation stress path and a one-dimensional stress path involving only vertical strains, the volumetric strains were divided by three based on the assumption that the strains are equal in the vertical and both horizontal directions. This assumption is not strictly correct because soil may exhibit anisotropy. However, agreement between the measurements and prediction is very good.

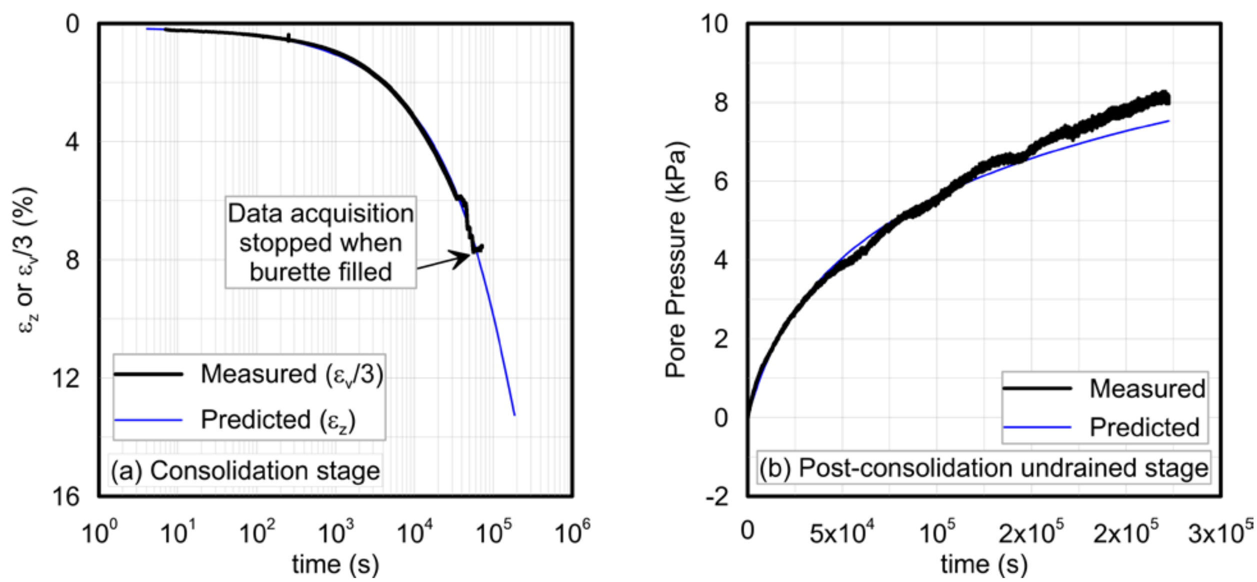

Figure 10. Sherman Island peat behavior: (a) measured versus predicted volumetric strain versus time for the consolidation stage; (b) pore pressure versus time during the postconsolidation undrained stage.

After closing the drainage tap, the clock was set to zero and pore pressure in the sample was monitored. The pore pressure increased with time, eventually reaching 8 kPa after about 250,000s when the test was terminated. Pore pressure was predicted by solving Eq. 12 for zero flow conditions, such that the terms associated with d^2u/dz^2 were set to zero. The predicted pore pressure increase agrees quite well with the measured pore pressure.

Having established that secondary compression can cause an increase in pore pressure when drainage is impeded, I now demonstrate that this mechanism can also occur for field conditions when the soil layer thickness is large enough to effectively impede drainage at the center for an adequate amount of time. For the example problem in Fig. 8, pore pressure isochrones are plotted at an average degree of consolidation near 10%, as shown in Fig. 11. Excess pore pressure is generated in the middle of the thicker layers because a significant amount of time is required for pore pressure to begin to dissipate. However, for the thinner layers, the rate of consolidation is fast enough that the excess pore pressure generated by secondary compression is negligible.

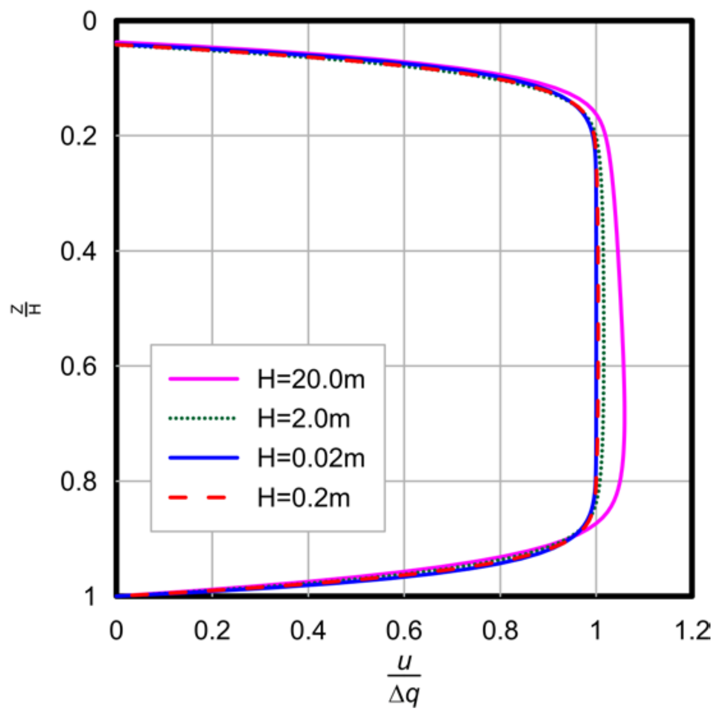

Figure 11. Isochrones at average degree of consolidation near 10% for the consolidation stage in Fig. 6.

An important consideration is that Fig. 11 presents a case in which the soil is initially normally consolidated. However, this is an unrealistic condition for natural soil deposits, even those that have not been mechanically loaded to a higher pressure. Secondary compression that occurs during the time required for the deposit to come into hydrostatic equilibrium would result in the void ratio being lower than the NCL, hence resulting in an overconsolidated condition. Therefore, deposits that have naturally aged are not likely to generate excess pore pressure due to secondary compression. Selecting an appropriate overconsolidation ratio therefore must consider the combined effects of mechanical pre-loading and secondary compression.

Conclusions

A nonlinear one dimensional implicit finite difference code for primary consolidation and secondary compression has been developed. Innovations associated with the code are (1) it is a publicly accessible web application, (2) it includes secondary compression simultaneously with primary consolidation by modeling the plastic volumetric strain rate due to secondary compression as a function of position in *e*-logσ_v' rather than making it a function of an arbitrary time reference, (3) nonlinear secondary compression behavior that has been observed for overconsolidated soils is accurately predicted, and (4) excess pore pressures generated by secondary compression for soils with impeded drainage is modeled, and agrees with experimental data.

Several limitations of the code must be considered for proper interpretation of analysis results. First, the code presented herein is one-dimensional, but field consolidation problems are typically three-dimensional and involve complex drainage boundary conditions. Second, as currently implemented the code permits only a single "uniform" soil layer, and does not permit users to input layered profiles. Many sites exhibit distinct geologic units that deviate from the boundary conditions currently permitted in the code. Third, the compressibility of soil is known to be nonlinear in e-$\log_{10}(\sigma_v')$ space (i.e., C_c depends on e), but C_c is assumed constant in the code. This is reasonable for many engineering problems, but can result in unreasonable results in some cases, particularly at high σ_v' where the predicted values of e may even become negative (a physically impossible condition). Fourth, the code predicts very low secondary compression rates for highly overconsolidated soil, which does not agree well with laboratory observations. Solving this problem lies beyond the scope of this manuscript, but the framework is amenable to future modifications to better match observed behavior. Fifth, the code permits only a single instantaneous application of vertical load, and assumes that the change in pore pressure is equal to the change in vertical total stress. Real problems often involve time-dependent loading conditions due to construction time-lines, and unsaturated soil conditions for which the change in vertical stress is not equal to the change in pore pressure. Finally, the code has not been compared with a wide range of experimental data, and doing so is beyond the scope of this manuscript. Future studies are being planned by the author, and hopefully the publicly available code will also be used by others to provide future validation. Due to these limitations engineers are encouraged to use judgment in interpreting their numerical predictions, and perhaps use a different code (such as those cited early in this paper) that is better suited to the particular problem at hand if any of the limitations are deemed unacceptable.

Acknowledgments

I would like to thank my colleagues Jonathan Stewart and Ali Shafiee for their input on the details of the consolidation code. I would like to thank Mandro Eslami for helping to set up the isotropic consolidation test on Sherman Island peat. Finally, I would like to thank the students in my advanced soil mechanics graduate course who served as guinea pigs for the code, and helped me work out many of the bugs. This work was performed as part of a research study funded by the California Department of Water Resources under contract number 4600010406. Any opinions, findings, and conclusions or recommendations expressed in this material are those of the author(s) and do not necessarily reflect the views of the California Department of Water Resources.

References

Barden, L (1965). “Consolidation of clay with non-linear viscosity, *Geotechnique*, 15(4), 345-362.

Bjerrum, L. (1967). “Engineering geology of Norweigan normally consolidated marine clays as related to settlements of buildings.” *Geotechnique,* 17(2) 81-118.

Borja, R.I. (1992). “Generalized creep and stress relaxation model for clays.” . *J. Geotechnical Engineering*, 118(11), 1765-1786.

Casagrande, A. (1936). “The determination of the preconsolidation load and its practical significance,” *Proceedings, 1st International Conference on Soil Mechanics and Foundation Engineering*, Cambridge, Mass., 60-64.

Crank, J., and Nicolson, P. (1947). “A practical method for numerical evaluation of solutions of partial differential equations of the heat conduction type.” *Proc. Camb. Phil. Soc.* 43(1), 50-67.

Fox, P.J., and Berles, J.D. (1997). “CS2: A piecewise-linear model for large strain consolidation.” *International Journal for Numerical and Analytical Methods in Geomechanics,* 21, 453-475.

Fox, P.J., Edil, T.B., and Lan, L.-T. (1992). “C_α/C_c concept applied to compression of peat.” J. Geotech. Eng., 118(8), 1256-1263.

Fox, P.J. (1999). “Solution charts for finite strain consolidation of normally consolidated clays.” *J. Geotech. Geoenviron. Eng.,* 125(10), 847-867.

Fox, P.J., and Pu, H. (2015). “Benchmark problems for large strain consolidation.” *J. Geotech. Geoenviron. Eng.*, 141(11).

Gibson, R.E., and Lo, K.Y. (1961). A theory of consolidation for soils exhibiting secondary compression. *Norwegian Geotechnical Institute*, Proc. 41, pp 3-15.

Handy, R.L., (2002). “First-order rate equations in geotechnical engineering.” *J. Geotech. Geoenviron. Eng.* 128(5), 416-425.

Kutter, B.L., and Sathialingam, N. (1992). “Elastic-viscoplastic modelling of the rate-dependent behavior of clays.” *Geotechnique*, 42(3), 427-441.

Lambrechts, J., Layhee, C., and Straub, N. (2004). “Analyzing surcharge needs to reduce secondary compression at embankment interfaces,” in Geotechnical Engineering for Transportation Projects, Geotechnical Special Publication No. 126, M.K. Yegian and E. Kavazanjian (eds), Vol. 2, pp. 2048-2057.

Leroueil, S. (2006). "The isotache approach. Where are we 50 years after its development by Professor Suklje? (2006 Prof. Suklje's Memorial Lecture." *Proc. 13th Danube-European Conference on Geotechnical Engineering, Ljubljana, pp. 55-88.*

Mesri, G., and Choi, Y.K. (1985). "Settlement analysis of embankments on soft clays." *J. Geotech. Eng.* 111(4), 441-464.

Mesri, G., Stark, T.D., Ajlouni, M.A., and Chen, C.S. (1997). "Secondary compression of peat with or without surcharging." *J. Geotech. Geoenviron. Eng.*, 123(5), 411-421.

Mesri, G., and Godlewski, P.M. (1977). "Time- and stress-compressibility interrelationship." *J. Geotech. Engrg. Div.,* ASCE, 103(5), 417-430.

Mesri, G., and Ajlouni, M. (2007). "Engineering properties of fibrous peat." *J. Geotech. Geoenviron. Eng.*, 133(7), 851-866.

Niemunis, A., and Krieg, S. (1996). "Viscous behavior of soil under oedometric conditions." *Canadian Geotechnical Journal*, 33, 159-168.

Perrone, V.J. (1998). "One dimensional computer analysis of simultaneous consolidation and creep of clay." PhD. Dissertation, Virginia Polytechnic Institute, 369 p.

Perzyna, P. (1963). "The constitutive equations for rate-sensitive plastic materials." *Quarterly of Applied Mathematics*, 20: 321-332.

Rajot, J.-P., (1992). "A theory for the time-dependent yielding and creep of clay." PhD Dissertation, Virginia Polytechnic Institute, 367 p.

Reinert, E., Stewart, J.P., Moss, R.E.S., and Brandenberg, S.J. (2014). "Dynamic Response of a Model Levee on Sherman Island Peat: A Curated Data Set." Earthquake Spectra, 30(2), 639-656.

Rocscience (2009). “Settle 3D Settlement and consolidation analysis theory manual.” Rocscience Inc. 52 p.

Shafiee, A. (2016). “Cyclic and post-cyclic behavior of Sherman Island peat.” PhD Dissertation, University of California, Los Angeles, 303 p.

Tavenas, F., Jean, P., Leblond, P., and Leroueil, S., (1983). "The Permeability of Natural Soft Clays. Part II: Permeability Characteristics," *Canadian Geotechnical Journal,* Vol. 20, No. 4, pp. 645-660.

Taylor, D.W. (1942). “Research on consolidation of clays.” *Massachusetts Institute of Technology,* Department of Civil and Sanitary Engineering, Serial 82, 147 p.

Taylor, D.W. (1948). *Fundamentals of Soil Mechanics*, Wiley, New York, 712 p.

Taylor, D.W. and Merchant, W. (1940). “A theory of clay consolidating accounting for secondary compression.” *J. Maths. And Physics,* 19:3, pp 167-185.

Terzaghi, K. (1925). “Erdbaumechanik auf Bodenphsikalischer Grundlage”, Franz Deuticke, Leipzig und Wein, 399 p. “Structure and Volume of Voids of Soils,” pp. 10-13 (translated by A. Casagrande) in Terzaghi (1960).

Terzaghi, K. (1960). *From Theory to Practice in Soil Mechanics*, Wiley, New York, 425 p.

Thomas, L.H. (1949), *Elliptic Problems in Linear Differential Equations over a Network*, Watson Sci. Comput. Lab Report, Columbia University, New York.

Yin, J.H., and Graham, J. (1996). “Elastic visco-plastic modeling of one-dimensional consolidation.” *Geotechnique*, 46(3), 515-527.

Appendix

The implicit algorithm requires evaluation of the partial derivatives in Eq. 14. The derivatives are provided below.

$$\frac{\partial R_{i,j}}{\partial u_{i,j}} = -\frac{a_{v_{i,j}}}{1+e_{i,j-1}} - \frac{k_{i,j}\cdot \Delta t}{\gamma_w \cdot \Delta z_{i,j}^2} \qquad (16)$$

$$\frac{\partial R_{i,j}}{\partial u_{i-1,j}} = \frac{0.5 \cdot \Delta t}{\gamma_w \cdot \Delta z_{i,j}^2} \left[k_{i,j} + 0.25 \left(k_{i-1,j} - k_{i+1,j} \right) \right] \tag{17}$$

$$\frac{\partial R_{i,j}}{\partial u_{i+1,j}} = \frac{0.5 \cdot \Delta t}{\gamma_w \cdot \Delta z_{i,j}^2} \left[k_{i,j} + 0.25 \left(k_{i+1,j} - k_{i-1,j} \right) \right] \tag{18}$$

$$\frac{\partial R_{i,j}}{\partial a_{v_{i,j}}} = -\frac{u_{i,j} - u_{i,j-1}}{1 + e_{i,j-1}} \tag{19}$$

$$\frac{\partial R_{i,j}}{\partial k_{i,j}} = \frac{0.5 \cdot \Delta t}{\gamma_w \cdot \Delta z_{i,j}^2} \left(u_{i-1,j} - 2.0 \cdot u_{i,j} + u_{i+1,j} \right) \tag{20}$$

$$\frac{\partial R_{i,j}}{\partial k_{i-1,j}} = \frac{0.125 \cdot \Delta t}{\gamma_w \cdot \Delta z_{i,j}^2} \left(u_{i-1,j} - u_{i+1,j} \right) \tag{21}$$

$$\frac{\partial R_{i,j}}{\partial k_{i+1,j}} = \frac{0.125 \cdot \Delta t}{\gamma_w \cdot \Delta z_{i,j}^2} \left(u_{i+1,j} - u_{i-1,j} \right) \tag{22}$$

$$\frac{\partial R_{i,j}}{\partial \sigma_{v_{i,j}}} = \frac{0.5 \cdot \Delta t \cdot C_c}{\sigma_{v_{i,j}} \cdot \ln(10) \cdot t_{ref} \cdot \left(1 + e_{i,j-1} \right)} \cdot \exp\left(\frac{e_{i,j} - e_{ref}}{\alpha} + \frac{C_c}{\alpha} \log\left(\frac{\sigma_{v_{i,j}}}{\sigma_v{}'_{c\alpha,ref}} \right) \right) \tag{23}$$

$$\frac{\partial R_{i,j}}{\partial e_{i,j}} = \frac{0.5 \cdot \Delta t}{t_{ref} \cdot \left(1 + e_{i,j-1} \right)} \exp\left(\frac{e_{i,j} - e_{c\alpha,ref}}{\alpha} + \frac{C_c}{\alpha} \log\left(\frac{\sigma_{v_{i,j}}}{\sigma_v{}'_{c\alpha,ref}} \right) \right) \tag{24}$$

$$\frac{\partial R_{i,j}}{\partial \Delta z_{i,j}} = -\frac{\Delta t}{\gamma_w \cdot \Delta z_{i,j}{}^3} \left[k_{i,j} \cdot \left(u_{i-1,j} - 2 \cdot u_{i,j} + u_{i+1,j} \right) + 0.25 \cdot \left(k_{i+1,j} - k_{i-1,j} \right) \cdot \left(u_{i+1,j} - u_{i-1,j} \right) \right] \tag{25}$$

$$\frac{\partial \sigma_{v_{i,j}}}{\partial u_{i,j}} = -1 \tag{26}$$

$$\frac{\partial k_{i,j}}{\partial e_{i,j}} = \frac{k_{ref} \cdot \ln(10)}{C_k} 10^{\frac{e_{i,j} - e_{k,ref}}{C_k}} \tag{27}$$

$$\frac{\partial k_{i-1,j}}{\partial e_{i-1,j}} = \frac{k_{ref} \cdot \ln(10)}{C_k} 10^{\frac{e_{i-1,j} - e_{k,ref}}{C_k}} \tag{28}$$

$$\frac{\partial k_{i+1,j}}{\partial e_{i+1,j}} = \frac{k_{ref} \cdot \ln(10)}{C_k} 10^{\frac{e_{i+1,j} - e_{k,ref}}{C_k}} \tag{29}$$

$$\frac{\partial k_{i,j}}{\partial u_{i,j}} = \frac{0.5 \cdot \ln(10) \cdot a_{v_{i,j}} \cdot k_{ref}}{C_k} \exp\left(\ln(10) \frac{e_{i,j-1} + a_{v_{i,j}} \left(u_{i,j} - u_{i,j-1} \right) - e_{k,ref}}{C_k} \right) \tag{30}$$

$$\frac{\partial e_{i,j}}{\partial u_{i,j}} = \frac{a_{v_{i,j}}}{1 + \frac{0.5 \cdot \Delta t}{t_{ref}} \exp\left(\frac{e_{i,j} - e_{c\alpha,ref}}{\alpha} + \frac{C_c}{\alpha} \log\left(\frac{\sigma_{v_{i,j}}}{\sigma_{vc\alpha,ref}} \right) \right)} \tag{31}$$

$$\frac{\partial e_{i,j}}{\partial u_{i,j}} = \frac{a_{v_{i-1,j}}}{1 + \frac{0.5 \cdot \Delta t}{t_{ref}} \exp\left(\frac{e_{i-1,j} - e_{c\alpha,ref}}{\alpha} + \frac{C_c}{\alpha} \log\left(\frac{\sigma_{v_{i-1,j}}}{\sigma_{vc\alpha,ref}} \right) \right)} \tag{32}$$

$$\frac{\partial e_{i,j}}{\partial u_{i,j}} = \frac{a_{v_{i+1,j}}}{1 + \frac{0.5 \cdot \Delta t}{t_{ref}} \exp\left(\frac{e_{i+1,j} - e_{c\alpha,ref}}{\alpha} + \frac{C_c}{\alpha} \log\left(\frac{\sigma_{v_{i+1,j}}}{\sigma_{vc\alpha,ref}} \right) \right)} \tag{33}$$

$$\frac{\partial a_{v_{i,j}}}{\partial \sigma_{v_{i,j}}} = \frac{C_c \left(\sigma_{v_{i,j}} - \sigma_{v_{i,j}} \ln\left(\frac{\sigma'_{v_{i,j}}}{\sigma'_{v_{i,j-1}}} \right) - \sigma_{v_{i,j-1}} \right)}{\sigma_{v_{i,j}} \cdot \ln(10) \cdot \left(\sigma_{v_{i,j}} - \sigma_{v_{i,j-1}} \right)^2} \qquad \text{if } \sigma_p'{}_{i,j} = \sigma_v'{}_{i,j-1}$$

$$\frac{\partial a_{v_{i,j}}}{\partial \sigma_{v_{i,j}}} = \frac{C_r \left(\sigma_{v_{i,j}} - \sigma_{v_{i,j}} \ln\left(\frac{\sigma'_{v_{i,j}}}{\sigma'_{v_{i,j-1}}} \right) - \sigma_{v_{i,j-1}} \right)}{\sigma_{v_{i,j}} \cdot \ln(10) \cdot \left(\sigma_{v_{i,j}} - \sigma_{v_{i,j-1}} \right)^2} \qquad \text{if } \sigma_p'{}_{i,j} > \sigma_v'{}_{i,j-1} + u_{i,j-1} - u_{i,j} \tag{34}$$

$$\frac{\partial a_{v_{i,j}}}{\partial \sigma_{v_{i,j}}} = \frac{C_c \left(\sigma_{v_{i,j}} - \sigma_{v_{i,j}} \ln\left(\frac{\sigma_{v_{i,j}}}{\sigma_{p_{i,j}}} \right) - \sigma_{v_{i,j-1}} \right) - C_r \cdot \sigma_{v_{i,j}} \cdot \ln\left(\frac{\sigma_{p_{i,j}}}{\sigma_{v_{i,j-1}}} \right)}{\sigma_{v_{i,j}} \cdot \ln(10) \cdot \left(\sigma_{v_{i,j}} - \sigma_{v_{i,j-1}} \right)^2} \qquad \text{otherwise}$$

$$\frac{\partial \Delta z_{i,j}}{\partial e_{i,j}} = \frac{\Delta z_{i,j-1}}{1 + e_{i,j-1}} \tag{35}$$

$$\frac{\partial e_{i,j}}{\partial \sigma_{v_{i,j}}} = \frac{\frac{0.5 \cdot C_c \cdot \Delta t}{t_{ref} \cdot \sigma_{v_{i,j}} \cdot \ln(10)} \exp\left(\frac{e_{i,j} - e_{c\alpha,ref}}{\alpha} + \frac{C_c}{\alpha} \log\left(\frac{\sigma_{v_{i,j}}}{\sigma_{vc\alpha,\mathrm{ref}}} \right) \right)}{1 + \frac{0.5 \cdot \Delta t}{t_{ref}} \exp\left(\frac{e_{i,j} - e_{c\alpha,ref}}{\alpha} + \frac{C_c}{\alpha} \log\left(\frac{\sigma_{v_{i,j}}}{\sigma_{vc\alpha,\mathrm{ref}}} \right) \right)} \tag{36}$$